Tuning the Intrinsic Anisotropy with Disorder in the CaKFe4As4 Superconductor

# Tuning the intrinsic anisotropy with disorder in $CaKFe_4As_4$ superconductor

D. Torsello,[1,2] G. A. Ummarino,[1,3] J. Bekaert,[4] L. Gozzelino,[1,2] R. Gerbaldo,[1,2]
M. A. Tanatar,[5,6] P. C. Canfield,[5,6] R. Prozorov,[5,6] and G. Ghigo[1,2]

[1]*Politecnico di Torino, Department of Applied Science and Technology, Torino 10129, Italy*
[2]*Istituto Nazionale di Fisica Nucleare, Sezione di Torino, Torino 10125, Italy*
[3]*National Research Nuclear University MEPhI (Moscow Engineering Physics Institute), Moskva 115409, Russia*
[4]*Department of Physics, University of Antwerp, Groenenborgerlaan 171, B-2020 Antwerp, Belgium*
[5]*Ames Laboratory, Iowa State University, Ames, Iowa 50011, USA*
[6]*Department of Physics & Astronomy, Iowa State University, Ames, Iowa 50011, USA*

(Dated: May 16, 2020)

We report on the anisotropy of the London penetration depth of $CaKFe_4As_4$, discussing how it relates to its electronic structure, and how it modifies under introduction of disorder, both chemically-induced (by Ni substitution) and irradiation-induced (by 3.5-MeV protons). Indeed, $CaKFe_4As_4$ is particularly suitable for the study of fundamental superconducting properties due to its stoichiometric composition, exhibiting clean-limit behavior in the pristine samples and having a fairly high critical temperature, $T_c \approx 35$ K. The London penetration depth $\lambda_L$ was measured with a microwave coplanar resonator technique that allowed us to deconvolve the anisotropic contributions $\lambda_{L,ab}$ and $\lambda_{L,c}$ and obtain the anisotropy parameter $\gamma_\lambda = \lambda_{L,c}/\lambda_{L,ab}$. The $\gamma_\lambda(T)$ found for the undoped pristine sample is in good agreement with previous literature and is here compared to *ab initio* density functional theory and Eliashberg calculations. The dependence of $\gamma_\lambda(T)$ on both chemical and irradiation-induced disorder is discussed to highlight which method is more suitable to decrease the direction dependence of electromagnetic properties whilst keeping a high critical temperature. Lastly, the relevance of an intrinsic anisotropy such as $\gamma_\lambda$ on application related anisotropic parameters (critical current, pinning) is discussed in light of the recent employment of $CaKFe_4As_4$ in the production of wires.

PACS numbers: pacs
Keywords: keywords

## I. INTRODUCTION

One of the reasons why iron based superconductors (IBSs) are very interesting for applications is their low anisotropy [1]. Despite their complex electronic structure, when compared to the cuprate family of high temperature superconductors their properties relevant to transport applications stand out as almost isotropic. However, a closer look reveals some unconventional behavior of the anisotropy of both penetration depth ($\gamma_\lambda = \lambda_c/\lambda_{ab}$) and upper critical field ($\gamma_H = H_{c2,ab}/H_{c2,c}$) and of their temperature dependence.

In conventional low-temperature single-band BCS superconductors, both $\gamma_\lambda$ and $\gamma_H$ are temperature independent and are equal, therefore the temperature dependence of the anisotropy has been considered for long as a signature of multi-band conductivity since it is the typical behavior of $MgB_2$ [2, 3]. Conversely, it was recently pointed out that it can also originate from anisotropy of the order parameter such as non s-wave character [4]. For the same historical reason, it is common belief that $\gamma_\lambda$ and $\gamma_H$, when temperature dependent, should vary in an opposite way. If $\gamma_\lambda$ increases with increasing temperature $\gamma_H$ should decrease (as in $MgB_2$ [3]) or vice versa (as in the 122 family of IBSs [5, 6]). The recent observation of both anisotropies increasing with increasing temperature in the case of $CaKFe_4As_4$ (CaK1144) [7] challenged this view and stimulated further theoretical and experimental investigations.

Moreover, the increasing interest on IBSs for the production of tapes, wires and coated conductors requires a full characterization of their anisotropic transport and pinning properties, that have been shown to be strongly related to intrinsic anisotropies such as $\gamma_\lambda$ [8]. Specifically, the anisotropy parameter that enters the anisotropic Ginzburg Landau (AGL) scaling relation for the angular dependent critical current was shown to behave just as $\gamma_\lambda$ for $MgB_2$ [9] and Fe(Se,Te) [8] and as $\gamma_H$ for $Ba(Fe,Co)_2As_2$ [10]. In addition, vortex pinning and anisotropy place fundamental restrictions on the current carrying capability of materials [11] and therefore a way to engineer them is required.

In this work, we determine experimentally the temperature dependence of the London penetration depth anisotropy in $CaKFe_4As_4$ crystals and how it is modified by chemical and ion-irradiation-induced disorder. Chemical disorder is studied by Ni for Fe substitution, that increases electron doping, whereas 3.5 MeV proton irradiation produces pointlike defects and small clusters [12]. The experimental data for the undoped pristine case is compared to *ab initio* density functional theory (DFT) and multiband Eliashberg theory calculations. The relevance of an intrinsic anisotropy such as $\gamma_\lambda$ on application related anisotropic parameters (critical current, pinning) is also discussed in light of the recent employment of CaK1144 in the production of wires

[13] and tapes [14]. In this respect, the ability to tune the anisotropy with disorder is a valuable tool for applications, and in the paper we discuss which method between doping and irradiation is more suitable to decrease the direction dependence of electromagnetic properties whilst keeping a high critical temperature.

## II. EXPERIMENTAL TECHNIQUES AND THEORETICAL METHODS

### A. Crystals preparation

High quality single crystals of $CaK(Fe_{1-x}Ni_x)_4As_4$ with analyzed doping levels of x=0, x=0.014 and x=0.037, were grown by high temperature solution growth out of FeAs flux [15]. The samples were cleaved and reduced to the form of thin rectangular plates with thicknesses ranging from 3 to about 35 $\mu$m, in the direction of the $c$-axis of the crystals, and width and length at least one order of magnitude larger.

### B. Penetration depth measurements

The London penetration depth was measured by means of a coplanar waveguide resonator (CPWR) technique that has already been applied to study other IBS crystals [16–19]. The resonator consists of an $YBa_2Cu_3O_{7-x}$ coplanar waveguide to which the sample is coupled. The whole resonance curve is recorded with a vector network analyzer, making it possible to track resonant frequency shifts and variations of the unloaded quality factor. This procedure gives access to the absolute value of the penetration depth and its temperature dependence after a calibration procedure is performed (full details in [20]). The sample is positioned on top of the central strip of the resonator in a region where the electric field vanishes, in a configuration with the rf magnetic field parallel to the $ab$-planes of the sample, i.e. to its broad face. Due to the finite size of the crystal and to the consequent demagnetization field, the measurements yields an effective penetration depth $\lambda_L$ that is a combination of the main components $\lambda_{L,ab}$ and $\lambda_{L,c}$. This combination depends on the geometry of the sample under consideration, and for this reason both components can be retrieved by measuring samples with significantly different aspect ratios.

Accordingly, and in the hypothesis that $\lambda_{L,ab} < c$ and $\lambda_{L,c} < a, b$ (where 2c, 2a, 2b are respectively the thickness, width and length of the samples), the fraction of penetrated volume can be estimated as $\lambda_{L,ab}/c + \lambda_{L,c}/a + \lambda_{L,c}/b$. Thus, the measured penetration depth can be expressed as:

$$\lambda_L = \lambda_{L,ab} + f_s \cdot \lambda_{L,c}, \qquad (1)$$

where $f_s = c \cdot (1/a + 1/b)$ is the sample shape factor. An example of the $\lambda_L$ deconvolution procedure for pristine undoped CaK1144 is given in Fig.1, where $\lambda_{L,ab}$ and $\lambda_{L,c}$ are extracted from the comparison of two crystals with very different shape factors (one order of magnitude). To improve precision, further crystals can be analyzed: we show in the inset of Fig.1 the best collapse of $\lambda_{L,ab}$ and $\lambda_{L,c}$ data from three crystals, resulting in the $\gamma_\lambda(T)$ reported in Fig.4 below.

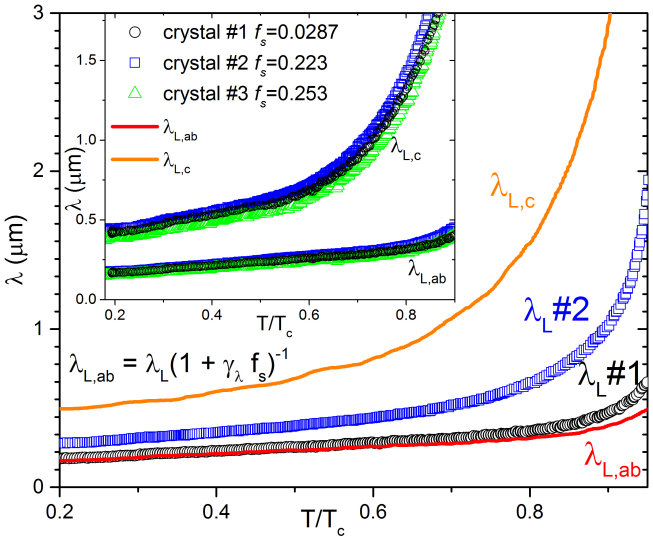


FIG. 1. Effective penetration depth of two crystals with a largely different shape factor and the resulting deconvolved $\lambda_{L,ab}$ and $\lambda_{L,c}$ contributions. The inset shows the best collapse of $\lambda_{L,ab}$ and $\lambda_{L,c}$ data from three crystals, resulting in the anisotropy factor discussed in Fig.4

### C. Proton irradiation

3.5-MeV proton irradiation was performed at the CN facility of the LNL laboratories of the Italian National Institute for Nuclear Physics (INFN), with the beam parallel to the $c$-axis of the crystals. The range of protons into the material was estimated to be about 66 $\mu$m by Monte Carlo simulations performed with the PHITS [21] and SRIM [22] codes within the Kinchin-Pease approach. The thickness of all investigated samples was much smaller than this value (maximum 35 $\mu$m), ensuring that proton implantation is avoided and that a rather homogeneous distribution of defects is achieved. CPWR measurements were carried out before and after each irradiation session.

### D. DFT calculations

Density functional theory (DFT) calculations, as implemented in ABINIT [23], were performed to obtain the Fermi surface of $CaKFe_4As_4$. We have used the Perdew-Burke-Ernzerhof (PBE) functional, in combination with projector augmented wave (PAW) atomic po-

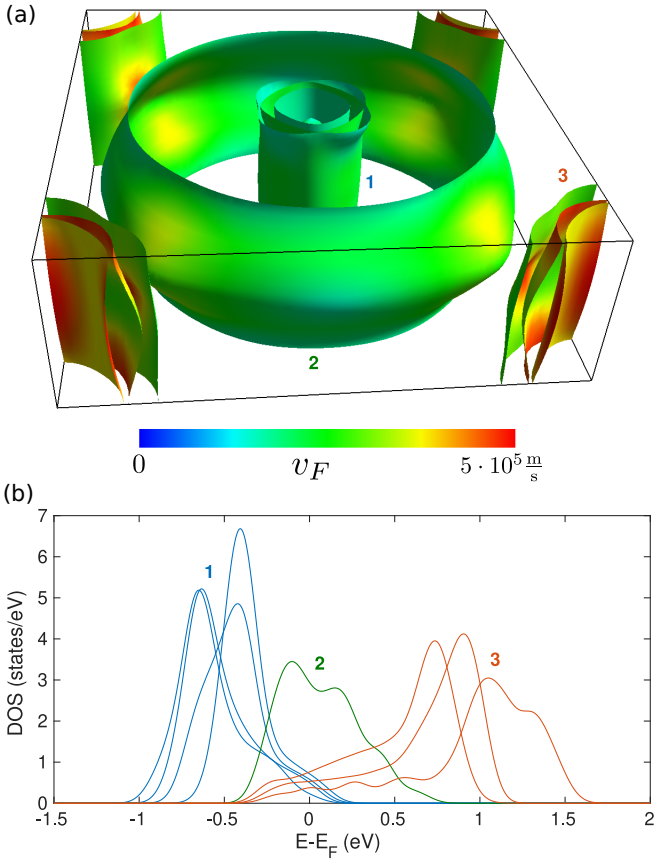


FIG. 2. (a) Fermi surface of $CaKFe_4As_4$ calculated using density functional theory, depicted in the Γ-centered Brillouin zone. (b) Band-resolved electronic density of states around the Fermi level. A total of eight bands are present, their characteristics suggesting that the system can essentially be described by a simplified three-component model.

tentials, taking into account Ca $3s^2 3p^6 4s^2$, K $3s^2 3p^6 4s^1$, Fe $3s^2 3p^6 3d^6 4s^2$ and As $3d^{10} 4s^2 4p^3$ as valence states. An energy cutoff of 15 Ha for the plane-wave basis was used, and a 20×20×6 Γ-centered Monkhorst-Pack **k**-point grid. The crystal structure was relaxed so that forces on each atom were below 1 meV/Å, yielding lattice parameters $a = 3.94$ Å and $c = 11.82$ Å.

The Fermi surface consists of five bands centered around Γ with hole character and three bands centered around M with electron character (Fig. 2(a)). One of the bands centered around Γ (the outer one) is much larger and more warped than the other four, suggesting that the system can be essentially described by a simplified three-component model (one equivalent electron band and two equivalent hole bands, one of which is the outer Γ band). To further characterize the superconducting components we have calculated the band-resolved density of states (DOS) using gaussian integration of the DFT Kohn-Sham eigenvalues with a width of 0.1 eV (Fig. 2(b)). The behavior of the band-resolved DOS supports the choice to employ a three-component model and allows calculating the component-resolved DOS at the Fermi level $N_i(0)$ (Tables I and II).

For each of the three components we also calculated the average Fermi velocities in the $ab$ and $c$ directions (Tables I and II) from the DFT Kohn-Sham eigenvalues ($\epsilon_{KS}$) using $\mathbf{v}_F = \hbar^{-1} \nabla_{\mathbf{k}} \epsilon_{KS}|_{\epsilon_{KS}=E_F}$, and subsequently averaging over the $ab$ and $c$ directions to capture the anisotropy.

### E. Eliashberg modelling

Eliashberg theory has been proven very helpful in the interpretation of experimental data for IBSs thanks to the possibility to take into account the spin fluctuation pairing mechanism and the multiband nature of these materials [24, 25]. London penetration depth can easily be calculated from the solution of the imaginary axis version of the Eliashberg equations. As suggested by the DFT calculations, we employed a three band model with pairing provided by antiferromagnetic spin fluctuations. The coupling constants are determined to reproduce the experimental critical temperature and the gap values measured by ARPES [26]. Figure 3 shows the

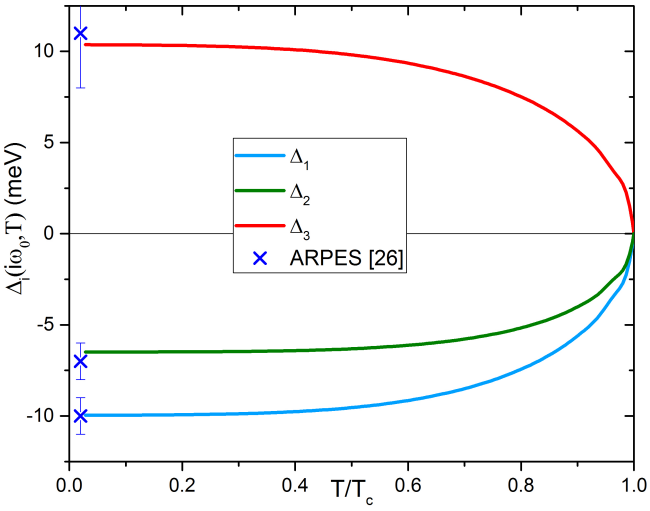


FIG. 3. Temperature dependence of the first value of the energy gaps of $CaKFe_4As_4$ obtained by the solution of the imaginary-axis Eliashberg equations. Crosses give the experimental ARPES data [26] for comparison.

temperature dependence of the energy gaps obtained by the solution of the imaginary-axis Eliashberg equations. All the details for the Eliashberg procedure to fix free parameters and calculate the London penetration depth are given elsewhere [24, 27]. In this specific case though, we do not consider the plasma frequency on each band as a free parameter but we obtain it from first principles. We use a simplified model in which gap anisotropy is not taken into account. However, it is still possible to evaluate anisotropic properties by employing the anisotropic

average Fermi velocity on each band obtained by DFT. In fact, the London penetration depth calculated by Eliashberg theory can be written as:

$$(\lambda_L^{El}(T))^{-2} = \sum_{i=1}^{3} (\frac{\omega_{p,i}}{c})^2 \pi T \times \Xi_i \qquad (2)$$

where $\omega_{p,i}$ is the bare plasma frequency on the $i$-th band that is related to the London penetration depth by $\omega_p = c/\lambda_L(0)$ only in the case of a clean uniform superconductor at $T = 0$ and in presence of negligible Fermi-liquid effects. If this is not the case, this relation is modified as $\omega_p^{sf} = c/\lambda_L(0)$, where $\omega_p^{sf}$ is the renormalized superfluid plasma frequency [28]. $\Xi_i$ gives the renormalization of the $i$-th band estimated by Eliashberg theory through the gap functions $\Delta_i(i\omega_n)$ and the renormalization functions $Z_i(i\omega_n)$ solution of the imaginary axis Eliashberg equations as:

$$\Xi_i = \sum_{n=-\infty}^{+\infty} \frac{\Delta_i^2(\omega_n) Z_i^2(\omega_n)}{[\omega_n^2 Z_i^2(\omega_n) + \Delta_i^2(\omega_n) Z_i^2(\omega_n)]^{3/2}} \qquad (3)$$

The bare, band resolved and direction ($\alpha$ and $\beta$) dependent plasma frequencies can be computed by first principles [28] (with the parameters values shown in Tab. I):

$$\omega_{p,i}^{\alpha\beta} = \sqrt{\frac{8\pi e^2}{\epsilon_o} N_i(0) \langle v_{F,\alpha} v_{F,\beta} \rangle_{FS_i}} \qquad (4)$$

where $\alpha$=$ab$,$c$, and $v_{F,ab}^2 = v_{F,a}^2 + v_{F,b}^2$. Accordingly, a bare anisotropy parameter can be calculated in the zero temperature limit as $\gamma_\lambda^{bare} = \omega_p^{ab}/\omega_p^c$, as discussed by Kogan [2], while a renormalized anisotropy parameter can be obtained through Eqs.2 and 3 as $\gamma_\lambda^{El} = \lambda_{L,c}^{El}/\lambda_{L,ab}^{El}$. The latter can also be studied as a function of temperature, starting from the temperature dependence of the gaps calculated within the Eliashberg approach.

TABLE I. Parameters for the three components model.

| Component | N $eV^{-1}$ | $\Delta(0)$ meV | $\langle v_{F,a(b)} \rangle$ m/s | $\langle v_{F,c} \rangle$ m/s |
|---|---|---|---|---|
| 1 | 2.03 | 11 | $1.08\times10^5$ | $0.21\times10^5$ |
| 2 | 2.94 | 7 | $1.16\times10^5$ | $0.90\times10^5$ |
| 3 | 1.67 | 11 | $2.08\times10^5$ | $0.37\times10^5$ |

## III. RESULTS AND DISCUSSION

### A. Pristine undoped CaK1144

The experimental $\gamma_\lambda(T)$ for the pristine undoped CaK1144 case is shown in Fig. 4 where it is also compared to literature data from $\mu$SR experiments [7] and

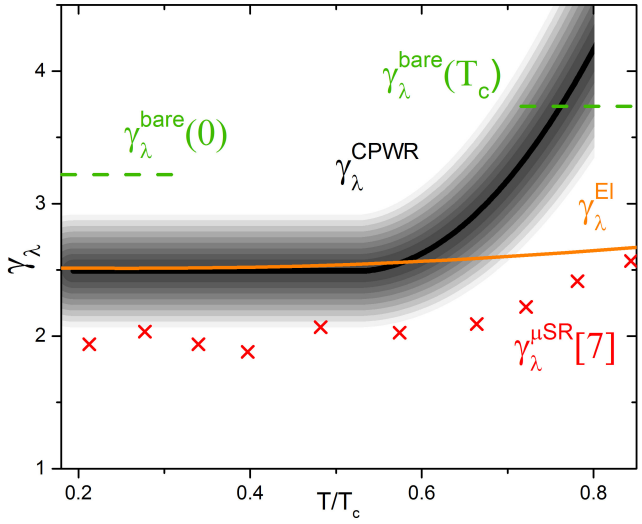


FIG. 4. Experimental anisotropy for the pristine undoped CaK1144, $\gamma_\lambda^{CPWR}$ (black solid line) with its estimated uncertainty (shaded area) compared to $\mu$SR data (red crosses) [7] and theoretical expectations, discussed in the text. $\gamma_\lambda^{bare}$ values (green) at $T$=0, $T_c$ are derived directly by *ab initio* DFT calculations, while $\gamma_\lambda(T)^{El}$ (orange solid line) takes into account the normalization given by the Eliashberg approach.

to calculated values. Experimental data are shown up to the reduced temperature where all the approximations discussed in Sect. II B are valid. The qualitative behavior from the two experimental techniques is comparable, with higher values in the CPWR case that can be ascribed to higher sample quality or to the higher frequency of the experimental probe that might reduce the scattering contribution [29]. As discussed above, thanks to the stoichiometric composition of undoped CaK1144 it has been possible to compute the bare low temperature anisotropy parameter from first principles as well as the renormalized one with its temperature dependence in the hypothesis that the gaps are isotropic. Both theoretical low temperature values are comparable with our experimental data: the bare value is slightly larger whereas the renormalized one is in remarkable agreement. The temperature dependence of the renormalized $\gamma_\lambda^{El}$ shows a modest upward curvature, reminiscent of the experimental behavior albeit quantitatively much smaller. From the comparison between the experimental and theoretical $\gamma_\lambda(T)$ it can be deduced that the gap and the full Fermi surface anisotropy (not included in the model) probably play a prominent role in the temperature dependence of the anisotropy parameter. This can be easily deduced by comparing the limiting behavior of $\gamma_\lambda(T)$ for $T \to 0$ and $T \to T_c$ discussed by Kogan *et al.* [2]. While for the low temperature limit only the Fermi velocities play a role, approaching the critical temperature a parameter that describes gap anisotropy ($\Omega$) enters the equation. This model has been recently extended to allow an approximate treatment of two-components systems with

anisotropic Fermi surfaces, starting from a few input parameters [4] that can easily be estimated starting from the DFT and Eliashberg data discussed above. For this purpose, from our DFT data we group the several bands contributions in just two components yielding the partial DOS and direction resolved Fermi velocities of each component and from the Eliashberg calculations we get an estimate of the gaps in the two component model by simply averaging the two contributions on the Γ bands. With the values summarized in Table II we get from Eq.s 31 and 32 in Ref. [4] that both $\gamma_\lambda$ and $\gamma_H$ increase with increasing temperature and that the variation is stronger for $H_{c2}$ than for $\lambda_L$, as experimentally observed [7] ($\gamma_\lambda(0)/\gamma_\lambda(T_c) \simeq 0.87$ and $\gamma_H(0)/\gamma_H(T_c) \simeq 0.8$). As a reference, we added to Fig.4 the value of $\gamma_\lambda^{bare}$ at $T_c$, as $\gamma_\lambda^{bare}(0)/0.87$.This value is close to the experimental ones at high temperatures, suggesting that indeed the Fermi surface anisotropy is crucial to address $\gamma_\lambda$ when approaching $T_c$.

TABLE II. Parameters for the two components model [4].

| Component | N $eV^{-1}$ | $\Delta(0)$ meV | $\langle v_{F,a(b)} \rangle$ m/s | $\langle v_{F,c} \rangle$ m/s |
|---|---|---|---|---|
| 1 | 4.97 | 11 | $1.12\times10^5$ | $0.60\times10^5$ |
| 2 | 1.67 | 9 | $2.08\times10^5$ | $0.37\times10^5$ |

### B. Disorder dependence of $\gamma_\lambda$

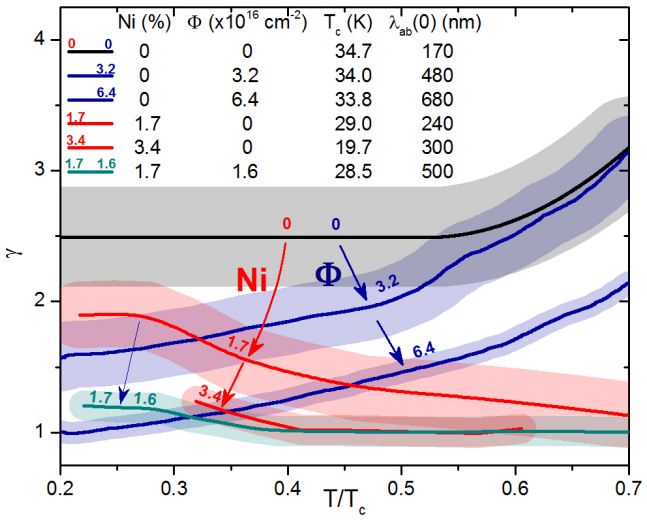


FIG. 5. Disorder dependence of the penetration depth anisotropy. Disorder is introduced by chemical substitution of Ni for Fe (red) and 3.5 MeV proton irradiation induced defects (blue) or a combination of the two (cyan).

Disorder is a valuable tool to tune anisotropy. Here we study the effects of two types of disorder: chemical substitution (Ni for Fe) and 3.5 MeV proton irradiation induced defects. This latter source of disorder produces mostly pointlike defects (vacancies, interstitials and Frenkel pairs) and small collision cascades with expected size of a few nm [12], which produce isotropic scattering of carriers and are then expected to reduce the anisotropy [2]. As visible from Fig. 5, both typologies of disorder reduces the overall anisotropy, but the temperature dependence is affected in opposite ways. With increasing irradiation fluence (and therefore defects concentration) $\gamma_\lambda(T)$ preserves its qualitative temperature behavior: increasing with temperature for the undoped case and decreasing with temperature for the 1.7% Ni doped case. On the other hand Ni substitution changes the temperature evolution from increasing to decreasing. This experimental evidence should be interpreted in light of the fact that substitution of Fe with Ni provides electron doping and its main consequence is to shift the Fermi level. However, these dopant ions also cause substantial scattering [29] (that is pair-breaking), just as the introduction of defects through irradiation does.
We find a decrease of anisotropy at low temperature both in irradiated and substituted samples, so we can ascribe this modification to the increase of scattering (a parameter not included in the models previously discussed). On the other hand, in the previous section, by comparing the two models, we discussed how in the $T \to T_c$ limit the gap anisotropy is predominant in determining $\gamma_\lambda$ . Therefore, the observed change of temperature dependence of $\gamma_\lambda$ as a consequence of Ni substitution is compatible with the expected modification of the band and gap structure.
Moreover, in combination with the decrease of critical temperature due to Ni doping or ion irradiation it is possible to discuss which method (or which combination) could be more advantageous to tune the anisotropy for a specific application.

### C. Relevance for applications

In the production of tapes, wires and coated conductors, the nature of grain-boundaries and the anisotropy of critical current are critical aspects. If the anisotropy of the material is too high and if precise grain boundaries orientation is required, a three-dimensionally controlled crystallites growth is needed, resulting in complicated fabrication processes and therefore high costs [30]. IBSs have the advantage, with respect to the cuprates, that the critical angle for grain orientation is quite large. This fact allows a wide space for improvement of the intergrain properties through the optimization of production processes such as texturing and application of pressure [31]. The intrinsic characteristics of these materials are not a fundamental limitation in this respect. This is especially true when considering the specific case of coated conductors that, although still a

young technology, are promising to achieve the critical current densities needed for practical appilcations [32]. However, intragrain properties on the other hand are not intrinsically as excellent as in the cuprates, and their optimization is pivotal for applications. For this reason the study of single crystals properties (where grain boundaries are absent), and the investigation of approaches for their optimization, is particularly relevant. Recently, a study on proton irradiation of single crystals of $CaKFe_4As_4$ has shown that the critical current of this materials can be strongly enhanced by introducing pointlike defects [33] making this material particularly interesting for applications. Moreover, despite the fact that IBSs are much less anisotropic than the cuprates, anisotropy values in the range of 2-5 can still result in a decrease of practical values of the superconducting parameters when external or stray fields are present (e.g. the engineering critical current of a coated conductor employed in the assembly of magnets), making the optimization of anisotropy a strong requirement for applications.

When flux-pinning models are considered to explain the field-angular dependence and anisotropy of the critical current density in IBSs, it turns out explicitly that the penetration depth anisotropy plays a role, together with the coherence length anisotropy [34]. In particular, $\gamma_\lambda$ directly enters into the elementary pinning force through the line energy term. The penetration depth anisotropy appears in the expressions for $j_c(\theta)$, with a relative weight depending on the pinning regime, shape of defects, and in general on the optimization of the matching between the vortex lattice and the defect matrix.

In the analysis of the angular dependence of the critical current $J_c(\theta)$, a valuable tool is the AGL approach [35] that allows one to scale $J_c(\theta)$ with an effective magnetic field. The scaling involves an anisotropy parameter $\gamma_s$ that, for a simple clean single-band case, should be the effective mass anisotropy that also coincides with the low temperature limit of the penetration depth anisotropy $\gamma_s = \gamma_m = \sqrt{m_c/m_{ab}} = \gamma_\lambda$.

Here we want to stress that $\gamma_\lambda$ does not take into account pinning (since it is measured below the critical field for vortex penetration) but only to the carriers properties and the way they interact with their surroundings, and for this reason we describe it as "intrinsic". Moreover, it might differ below $T_c$ from $\sqrt{m_c/m_{ab}}$ of the clean system due to scattering, and since it also depends on fine details of the pairing, multi-band nature and structure of the Fermi surface [4].

However, the AGL scaling approach has been shown to work well also for multiband systems [34] with $\gamma_s$ found to follow the temperature behavior of intrinsic anisotropies such as $\gamma_\lambda$ for $MgB_2$ [9] and Fe(Se,Te) [8] and as $\gamma_H$ for $Ba(Fe,Co)_2As_2$ [10]. A similar relation between the AGL anisotropy and the intrinsic anisotropy of the penetration depth, although only qualitative, has been observed also for other systems such as the 1111 [36] and the 111 [37] IBSs families. All these observations, together with the quantitative relations valid for simplified and limiting cases, strongly suggest that the intrinsic anisotropy has a strong correlation with the practical ones to be optimized for applications. A correct application of the AGL scaling with $\gamma_s$ estimated by $\gamma_\lambda$ could yield useful information about the pinning regime in the material [8], another essential aspect for applications.

For these reasons the study of $\gamma_\lambda$ and of the possible approaches to tune it, acquires particular relevance for the application oriented investigation of IBSs.

In light of the discussion above, the experimental data summarized in Fig. 5 suggests that ion irradiation might be advantageous with respect to chemical doping for tuning the anisotropy. The low temperature value of $\gamma_\lambda$ can be reduced significantly with a relatively low proton dose that has a minimal influence on the critical temperature ($\gamma_\lambda(T \simeq 5K) \simeq 1$ with a decrease of $T_c$ of less than 1 K, see the table in Fig.5). Moreover, it has been shown that ion irradiation has a beneficial effect on the critical current of CaK1144 tapes: 3 MeV proton irradiation with a dose yielding a comparable decrease of $T_c$ to the one discussed here resulted in an increase of $J_c$ close to 500% at 2 K [38]. Comparable results were also found on single crystals from the same source as in this study irradiated with 3 MeV protons [33]. Interestingly, the irradiation dose that yielded the maximum increase of critical current density caused a reduction of $T_c$ very close to the one we observe in the crystals that show a $\gamma_\lambda$ at low temperature equal to 1 (isotropic behavior). It should be noted that the decrease of the anisotropy is achieved at the expenses of an increased absolute value of $\lambda_L$. In principle this increase is detrimental for high currents and thermal fluctuations but, as just discussed, the critical current is found to increase thanks to the contribution of additional pinning. Also thermal fluctuations are not expected to play a critical role in applications, since a four-fold increase of $\lambda_L$ would result in a width of the critical fluctuations regime smaller than 1 K (estimated using the Ginzburg number [39]), far from the expected working conditions.

The combination of all these results (namely the small decrease of $T_c$, the increase of penetration depth and the advantageouses increase of critical current and decrease of anisotropy) strongly indicates that proton irradiation might be extremely useful in the optimization of $CaKFe_4As_4$ properties for practical applications. With this respect, it is noteworthy that recently several steps towards the applicability of ion irradiation in the commercial production of coated conductors was reported [40–42]. The proton irradiation used in this work and the irradiations with larger ions at moderate energies compatible with commercial production share a similar typology of defects: in both cases small clusters and point defects are introduced.

In addition, it has been pointed out that keeping the stoichiometric composition of CaK1144 is by itself a

strong advantage in the production process of wires and tapes [11], and ion irradiation allows to tune several properties whilst keeping fixed the stoichiometry.

## IV. CONCLUSIONS

We reported on the anisotropy of the London penetration depth of $CaKFe_4As_4$, experimentally evaluated by means of a microwave coplanar-waveguide-resonator technique, compared to expectations based on DFT *ab initio* calculations and Eliashberg modeling. The penetration depth anisotropy found for the undoped pristine crystals is in fairly good agreement with previous $\mu$SR experiments [7], and with theoretical predictions. Indeed, it results from Fig.4 that both experimental evaluations of $\gamma_\lambda(T)$ (from CPWR and $\mu$SR) and both calculated ones (from bare DFT and renormalized one, in three-gap and two-gap approximations) show increase with temperature and comparable absolute values. More in detail, a remarkable agreement has been found between the experimental low-temperature anisotropy and the value calculated from DFT with an Eliashberg renormalization within a three-band approach ($\gamma_\lambda(0) \approx 2.5$). On the contrary, the experimental $\gamma_\lambda(T)$ cannot be reproduced well at temperatures approaching $T_c$ by the Eliashberg model, where the gap and Fermi surface anisotropy are not accounted for. A simple two-component model that includes Fermi surface anisotropy [4] yields a stronger temperature dependence of the anisotropy parameter, suggesting that a fully anisotropic Eliashberg treatment - beyond the aims of this work - could fully capture the experimentally observed behavior.

The dependence of $\gamma_\lambda(T)$ on both chemical and irradiation-induced disorder has been studied. Both kinds of disorder resulted in a general decrease of the intrinsic anisotropy, but with peculiar features. While irradiation defects mainly act at low temperatures, preserving the increasing temperature dependence, doping with Ni on the Fe site causes a decreasing $\gamma_\lambda(T)$ temperature dependence. This fact, in combination with the employed models, suggests that Ni substitution modifies more strongly than irradiation-induced defects the electronic and gap structure, while interband scattering is the most likely candidate to explain the decrease of $\gamma_\lambda$ at low temperature.

We obtained, in particular with a combination of doping and irradiation, crystals with virtually isotropic behavior. On the other hand, if one aims at discussing which method is the most convenient to decrease $\gamma_\lambda(T)$ in view of practical applications, doping and irradiation effects on the other key parameters should be taken into account: doping causes a fast decrease of the critical temperature, while irradiation mainly affects $\lambda_{L,ab}(0)$. In the case of tapes or wires, the second method could be preferred, since it simultaneously assures low anisotropy, very low decrease of $T_c$ and a huge increase of the critical current density through flux pinning.

## ACKNOWLEDGMENTS

This work was partially supported by the Italian Ministry of Education, University and Research (Project PRIN HIBiSCUS, Grant No. 201785KWLE). J. B. acknowledges support of a postdoctoral fellowship of Research Foundation-Flanders (FWO). The computational resources and services used for the first-principles calculations in this work were provided by the VSC (Flemish Supercomputer Center), funded by the FWO and the Flemish Government department EWI. Work done at Ames Lab was supported by the U.S. Department of Energy, Office of Basic Energy Science, Division of Materials Sciences and Engineering. Ames Laboratory is operated for the U.S. Department of Energy by Iowa State University under Contract No. DE-AC02-07CH11358. G.A.U. acknowledges the support from the MEPhI Academic Excellence Project (Contract No. 02.a03.21.0005).

[1] M. Putti, I. Pallecchi, E. Bellingeri, M. R. Cimberle, M. Tropeano, C. Ferdeghini, A. Palenzona, C. Tarantini, A. Yamamoto, J. Jiang, J. Jaroszynski, F. Kametani, D. Abraimov, A. Polyanskii, J. D. Weiss, E. E. Hellstrom, A. Gurevich, D. C. Larbalestier, R. Jin, B. C. Sales, A. S. Sefat, M. A. McGuire, D. Mandrus, P. Cheng, Y. Jia, H. H. Wen, S. Lee, and C. B. Eom, Superconductor Science and Technology **23**, 034003 (2010).

[2] V. G. Kogan, Phys. Rev. B **66**, 020509 (2002).

[3] J. D. Fletcher, A. Carrington, O. J. Taylor, S. M. Kazakov, and J. Karpinski, Phys. Rev. Lett. **95**, 097005 (2005).

[4] V. G. Kogan, R. Prozorov, and A. E. Koshelev, Phys. Rev. B **100**, 014518 (2019).

[5] R. Khasanov, D. V. Evtushinsky, A. Amato, H.-H. Klauss, H. Luetkens, C. Niedermayer, B. Büchner, G. L. Sun, C. T. Lin, J. T. Park, D. S. Inosov, and V. Hinkov, Phys. Rev. Lett. **102**, 187005 (2009).

[6] M. A. Tanatar, N. Ni, C. Martin, R. T. Gordon, H. Kim, V. G. Kogan, G. D. Samolyuk, S. L. Bud'ko, P. C. Canfield, and R. Prozorov, Phys. Rev. B **79**, 094507 (2009).

[7] R. Khasanov, W. R. Meier, S. L. Bud'ko, H. Luetkens, P. C. Canfield, and A. Amato, Phys. Rev. B **99**, 140507 (2019).

[8] K. Iida, J. Hänisch, E. Reich, F. Kurth, R. Hühne, L. Schultz, B. Holzapfel, A. Ichinose, M. Hanawa, I. Tsukada, M. Schulze, S. Aswartham, S. Wurmehl, and B. Büchner, Phys. Rev. B **87**, 104510 (2013).

[9] E. M. Choi, H.-J. Kim, S. K. Gupta, P. Chowdhury, K. H. P. Kim, S.-I. Lee, W. N. Kang, H.-J. Kim, M.-H. Jung, and S.-H. Park, Phys. Rev. B **69**, 224510 (2004).

[10] J. Hanisch, K. Iida, S. Haindl, F. Kurth, A. Kauffmann, M. Kidszun, T. Thersleff, J. Freudenberger, L. Schultz, and B. Holzapfel, IEEE Transactions on Applied Superconductivity **21**, 2887 (2011).

[11] Z. Cheng, C. Dong, H. Huang, S. Liu, Y. Zhu, D. Wang, V. Vlasko-Vlasov, U. Welp, W.-K. Kwok, and Y. Ma, Superconductor Science and Technology **32**, 015008 (2018).

[12] M. P. Smylie, M. Leroux, V. Mishra, L. Fang, K. M. Taddei, O. Chmaissem, H. Claus, A. Kayani, A. Snezhko, U. Welp, and W.-K. Kwok, Phys. Rev. B **93**, 115119 (2016).

[13] S. Pyon, D. Miyawaki, I. Veshchunov, T. Tamegai, K. Takano, H. Kajitani, N. Koizumi, and S. Awaji, Applied Physics Express **11**, 123101 (2018).

[14] Z. Cheng, S. Liu, C. Dong, H. Huang, L. Li, Y. Zhu, S. Awaji, and Y. Ma, Superconductor Science and Technology **32**, 105014 (2019).

[15] W. R. Meier, T. Kong, U. S. Kaluarachchi, V. Taufour, N. H. Jo, G. Drachuck, A. E. Böhmer, S. M. Saunders, A. Sapkota, A. Kreyssig, M. A. Tanatar, R. Prozorov, A. I. Goldman, F. F. Balakirev, A. Gurevich, S. L. Bud'ko, and P. C. Canfield, Phys. Rev. B **94**, 064501 (2016).

[16] G. Ghigo, G. A. Ummarino, L. Gozzelino, R. Gerbaldo, F. Laviano, D. Torsello, and T. Tamegai, Sci. Rep. **7**, 13029 (2017).

[17] G. Ghigo, D. Torsello, R. Gerbaldo, L. Gozzelino, F. Laviano, and T. Tamegai, Supercond. Sci. Technol. **31**, 034006 (2018).

[18] G. Ghigo, D. Torsello, G. A. Ummarino, L. Gozzelino, M. A. Tanatar, R. Prozorov, and P. C. Canfield, Phys. Rev. Lett. **121**, 107001 (2018).

[19] G. Ghigo, D. Torsello, L. Gozzelino, T. Tamegai, I. S. Veshchunov, S. Pyon, W. Jiao, G.-H. Cao, S. Y. Grebenchuk, I. A. Golovchanskiy, V. S. Stolyarov, and D. Roditchev, Phys. Rev. Research **1**, 033110 (2019).

[20] G. Ghigo, G. A. Ummarino, L. Gozzelino, and T. Tamegai, Phys. Rev. B **96**, 014501 (2017).

[21] T. Sato, K. Niita, N. Matsuda, S. Hashimoto, Y. Iwamoto, S. Noda, T. Ogawa, H. Iwase, H. Nakashima, T. Fukahori, K. Okumura, T. Kai, S. Chiba, T. Furuta, and L. Sihver, J. Nucl. Sci. Technol. **50**, 913 (2013).

[22] J. F. Ziegler, M. Ziegler, and J. Biersack, Nucl. Instrum. Meth. B **268**, 1818 (2010).

[23] X. Gonze, F. Jollet, F. Abreu Araujo, D. Adams, B. Amadon, T. Applencourt, C. Audouze, J.-M. Beuken, J. Bieder, A. Bokhanchuk, E. Bousquet, F. Bruneval, D. Caliste, M. Ct, F. Dahm, F. Da Pieve, M. Delaveau, M. Di Gennaro, B. Dorado, C. Espejo, G. Geneste, L. Genovese, A. Gerossier, M. Giantomassi, Y. Gillet, D. Hamann, L. He, G. Jomard, J. Laflamme Janssen, S. Le Roux, A. Levitt, A. Lherbier, F. Liu, I. Lukaevi, A. Martin, C. Martins, M. Oliveira, S. Ponc, Y. Pouillon, T. Rangel, G.-M. Rignanese, A. Romero, B. Rousseau, O. Rubel, A. Shukri, M. Stankovski, M. Torrent, M. Van Setten, B. Van Troeye, M. Verstraete, D. Waroquiers, J. Wiktor, B. Xu, A. Zhou, and J. Zwanziger, Comput. Phys. Commun. **205**, 106 (2016).

[24] D. Torsello, G. A. Ummarino, L. Gozzelino, T. Tamegai, and G. Ghigo, Phys. Rev. B **99**, 134518 (2019).

[25] G. A. Ummarino, D. Daghero, M. Tortello, and R. S. Gonnelli, Journal of Superconductivity and Novel Magnetism **24**, 247 (2011).

[26] D. Mou, T. Kong, W. R. Meier, F. Lochner, L.-L. Wang, Q. Lin, Y. Wu, S. L. Bud'ko, I. Eremin, D. D. Johnson, P. C. Canfield, and A. Kaminski, Phys. Rev. Lett. **117**, 277001 (2016).

[27] D. Torsello, G. A. Ummarino, R. Gerbaldo, L. Gozzelino, and G. Ghigo, Journal of Superconductivity and Novel Magnetism (2019), 10.1007/s10948-019-05368-2.

[28] O. V. Dolgov, A. A. Golubov, and D. Parker, New Journal of Physics **11**, 075012 (2009).

[29] D. Torsello, K. Cho, K. R. Joshi, S. Ghimire, G. A. Ummarino, N. M. Nusran, M. A. Tanatar, W. R. Meier, M. Xu, S. L. Bud'ko, P. C. Canfield, G. Ghigo, and R. Prozorov, Phys. Rev. B **100**, 094513 (2019).

[30] H. Hosono, A. Yamamoto, H. Hiramatsu, and Y. Ma, Materials Today **21**, 278 (2018).

[31] S. Pyon, T. Suwa, A. Park, H. Kajitani, N. Koizumi, Y. Tsuchiya, S. Awaji, K. Watanabe, and T. Tamegai, Superconductor Science and Technology **29**, 115002 (2016).

[32] K. Iida, H. Sato, C. Tarantini, J. Hänisch, J. Jaroszynski, H. Hiramatsu, B. Holzapfel, and H. Hosono, Scientific reports **7**, 39951 (2017).

[33] N. Haberkorn, M. Xu, W. R. Meier, S. Suárez, S. L. Bud'ko, and P. C. Canfield, Superconductor Science and Technology **33**, 025008 (2020).

[34] C. J. van der Beek, M. Konczykowski, and R. Prozorov, Superconductor Science and Technology **25**, 084010 (2012).

[35] G. Blatter, V. B. Geshkenbein, and A. I. Larkin, Phys. Rev. Lett. **68**, 875 (1992).

[36] C. Tarantini, K. Iida, J. Hänisch, F. Kurth, J. Jaroszynski, N. Sumiya, M. Chihara, T. Hatano, H. Ikuta, S. Schmidt, *et al.*, Scientific reports **6**, 36047 (2016).

[37] M. Kończykowski, C. J. van der Beek, M. A. Tanatar, V. Mosser, Y. J. Song, Y. S. Kwon, and R. Prozorov, Phys. Rev. B **84**, 180514 (2011).

[38] A. Takahashi, S. Pyon, S. Okayasu, S. Ishida, A. Iyo, H. Eisaki, M. Imai, H. Abe, T. Terashima, and T. Tamegai, Journal of Physics: Conference Series **1293**, 012013 (2019).

[39] L. Salasnich, A. A. Shanenko, A. Vagov, J. A. Aguiar, and A. Perali, Phys. Rev. B **100**, 064510 (2019).

[40] M. W. Rupich, S. Sathyamurthy, S. Fleshler, Q. Li, V. Solovyov, T. Ozaki, U. Welp, W.-K. Kwok, M. Leroux, A. E. Koshelev, *et al.*, IEEE Transactions on Applied Superconductivity **26**, 1 (2016).

[41] M. Leroux, K. J. Kihlstrom, S. Holleis, M. W. Rupich, S. Sathyamurthy, S. Fleshler, H. Sheng, D. J. Miller, S. Eley, L. Civale, *et al.*, Applied Physics Letters **107**, 192601 (2015).

[42] T. Ozaki, L. Wu, C. Zhang, W. Si, Q. Jie, and Q. Li, Superconductor Science and Technology **31**, 024002 (2018).